Free-Space Micro-Graphics with Electrically Driven Levitated Light Scatterers

Johann Berthelot, Nicolas Bonod

Free-Space Micro-Graphics with Electrically Driven Levitated Light Scatterers

Johann Berthelot, Nicolas Bonod

Free-Space Micro-Graphics with Electrically Driven Levitated Light Scatterers

JOHANN BERTHELOT[1,*] AND NICOLAS BONOD[1,*]

[1] Aix Marseille Univ, CNRS, Centrale Marseille, Institut Fresnel, Marseille, France
[*] Corresponding author: johann.berthelot@fresnel.fr, nicolas.bonod@fresnel.fr

Compiled January 25, 2019

Levitation of optical scatterers provides a new mean to develop free-space volumetric displays. The principle is to illuminate a levitating particle displaced at high velocity in three dimensions (3D) to create images based on persistence of vision (POV). Light scattered by the particle can be observed all around the volumetric display and therefore provides a true 3D image that does not rely on interference effects and remains insensitive to the angle of observation. The challenge is to control with a high accuracy and at high speed the trajectory of the particle in three dimensions. Here we use electrically driven planar Paul traps (PPTs) to control the trajectory of electrically charged particles. A single gold particle colloid is manipulated in three dimensions through AC and DC electrical voltages applied to a PPT. Electric voltages can be modulated at high frequencies (150 kHz) and allow for a high speed displacement of particles without moving any other system component. The optical scattering of the particle in levitation yields free-space images that are imaged with conventional optics. The trajectory of the particle is entirely encoded in the electric voltage and driven through stationary planar electrodes. We show in this paper, the proof-of-concept for the generation of 3D free space graphics with a single electrically scanned particle.

http://dx.doi.org/10.1364/ao.XX.XXXXXX

1. INTRODUCTION

Levitation of nano-objects is a fascinating area of science that aims at trapping and manipulating nano-objects without physical contact. Different techniques can be used to trap nano-objects, among which optical tweezers [1–5] or acoustic traps [6–8].

Recently, optical scatterers in levitation reveal as competing alternative to holography to yield volumetric images. Different systems have been proposed to provide free-space 3D imaging [9–12]. A major breakthrough was achieved in 2018 by the use of photophoretic traps [13]. Such traps use strong gradients in temperature around a lossy particle illuminated by a tightly focused laser beam. This trapping mechanism allows to trap particles in the range of a few micrometers up to hundreds of micrometers. This technique was shown to yield high quality centimeter-sized images. The optical trap is scanned with galvanometric mirrors that rely on a mechanical displacement of optical components. Here we show that immobilized planar point Paul traps can scan particles in a 3D space with AC and DC voltages only. The particle trajectory can be fully driven electrically without requiring any physical displacement of any component of the system.

Radio-frequency (RF) traps have been widely investigated to trap and control ions [14] and they are emerging in nano and microsciences as versatile tools to manipulate nano/micro-objects [15–21]. They rely on the use of a time varying electrical field applied on a special arrangement of electrodes forming an electrostatic potential featuring a saddle shape. RF traps operate with electrically charged nano/micro objects. This step is usually performed with the use of an electrospray ionization system (ESI) [22]. Conventional RF traps are bulky systems that offer low optical access, require high voltages and specific machining facilities. In the 2000's, the extension of this trap configuration into planar geometry has offered novel opportunities with levitation of electrically charged objects [23–25]. Besides weaker electric voltages required to trap objects, planar electrodes printed on the same plane offer an open access to easily detect and excite the levitated object with optical beams. Another advantage is related to the fabrication. Such systems are easily fabricated with conventional optical lithography or laser etching. The high stability of PPTs was unveiled in 2016 by translating and rotating PPTs while keeping particles trapped in levitation in air [26]. We show in this study that PPTs are highly suited to yield free-space images by manipulating and displacing individual optical scatterers by plugging the trajectory of particles into AC and DC voltages applied to stationary PPTs.

2. RESULTS AND DISCUSSION

A typical example of PPT is presented in Fig.1(a). The dimensions of the different electrodes are 0.7 mm in diameter for the inner electrode and 3 mm in diameter for the outer electrode. They were fabricated on a commercial Printed Circuit Board (PCB). It consists of two inner and outer ring electrodes surrounded by four compensation DC electrodes. The whole PPT has a size of 10×10 mm^2. Typically this PPT geometry requires oscillating fields in the kHz range with an amplitude of hundreds of volts. Connections are made underneath the planar PCB. By polarizing the different electrodes, either with DC or

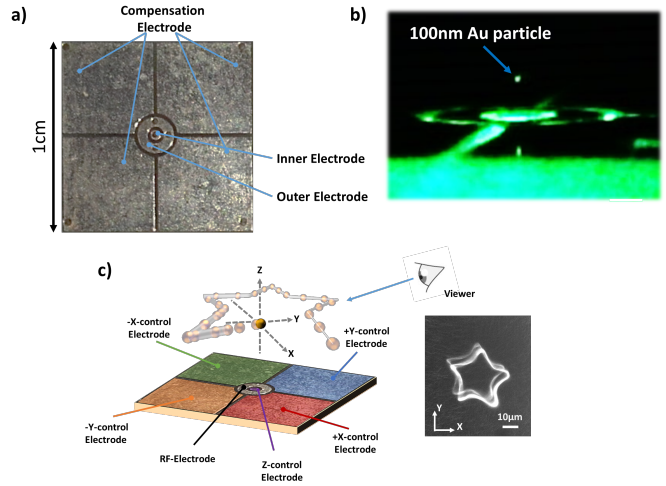

Fig. 1. Planar Paul traps. (a) Photography of a surface electrode trap used in this study. It is composed of different electrodes: inner electrode, RF electrode and 4 compensation DC electrodes. (b) Photography of a 100nm gold particle put in levitation with the PPT presented in (a). (c) Schematic illustration of the electrically driven motion of the particles. Each compensation electrode is used to control a $-Ox$, $+Ox$, $-Oy$, $+Oy$ direction. The displacement value is related to the amplitude of the applied electric field. The trajectory along the z axis is controlled with the inner electrode. Insert on the right is a free-space 2D image of a star obtained with our PPT.

AC voltage, it is possible to trap a single nano-object with a high stability (cf. Fig.1(b)). The four compensation electrodes add external parameters to displace the object in the plane while the inner electrode controls the out-of-plane displacement. The motion of the object is then driven depending of the configuration and the applied voltage amplitude of the different fields, *i.e.* AC or DC voltage. An important point is that all the AC voltages must be applied with the same frequency [26]. The circuit configuration used in this study is illustrated in Fig.1c. Thanks to this system, the trajectory of the particle can therefore be driven by directly encoding the amplitude in function of the position and applied to the electrodes by analog outputs. The speed and the precision of the driven motion are then strictly dependent of the electronic systems, *i.e.* bandwidth and resolution. In our experiments we used an electronic card from National Instrument (NI PCIe-7841R).

In the case where no driven electric field is applied, and taking into account the background pressure, the motion of the trapped particle can be predicted by solving the Mathieu equations [27]:

$$\frac{d^2u}{dy^2} + \mu\frac{du}{dy} + (a_u - 2q_u\cos 2y)u = 0, \quad \textbf{(1)}$$

where u denotes either the z or the r coordinate of the trapped particle. The dimensionless parameters a_u, q_u and μ are defined as follows:

$$a_u = 16\frac{Q}{M}\frac{V_{DC}}{\Omega^2}f(r,z), q_u = 8\frac{Q}{M}\frac{V_{AC}}{\Omega^2}f(r,z), \mu = 36\frac{\eta}{\rho d^2\Omega}. \quad \textbf{(2)}$$

. The dimensionless parameter y is related to time by $y = \Omega t/2$, where Ω is the frequency of the electrical field. By solving numerically Eq.1 for each direction of space, *i.e.* r and z, we can obtain the solutions depending on the dimensionless parameters a_u and q_u leading to a stable trap. A stable 3D trapping occurs when the different solutions in r and z overlap.

The function $f(r,z)$ depends on the geometry of the electrodes, d is the diameter of the particle, ρ is the density of the material and η the viscosity of the medium. We can remark that both parameters a_u and b_u depend on the charge-to-mass ratio Q/M and that a_u depends on a static voltage applied on the electrode. Particles are commonly trapped with a pure oscillating field, V_ac, without any static field V_dc, meaning that $a_u = 0$. a_u and q_u depend on the spatial parameter $u = r, z$ but due to the symmetry of the electrode, a_z and a_r are linked *via* the relation $a_z = -2a_r$. The same relation occurs for the q_u parameters, $q_z = -2q_r$. Solving Eq.1 provides the r or z coordinates leading to a stable position of the particle in the trap. For that purpose, a second-order Runge-Kutta method is implemented. This allows us to plot the stability diagram of the PPT as a function of the dimensionless parameters a_u, q_u for a given μ. μ is taken equal to 30 in air and equal to 0 in vacuum. We consider the case of an AC voltage with 1kHz frequency, 70 V amplitude and a 100 nm diameter gold particle (typical value used in the experiment). The solutions r and z are calculated with respect to a_u, q_u and the resulting stable 3D trapping solutions are plotted in Fig.2(a) as functions of a and q. We can clearly see that the domain of stability is much larger in air (in blue) than under vacuum (in orange). This result highlights the interest of electrostatic traps to operate in ambient conditions. We can observe in Fig.2 a large range of stable solutions for a wide range of a and q values, *i.e.* for a wide range of object sizes with different charge-to-mass ratio Q/m, for the same field applied. This also means that RF traps can operate for an even wider range of object sizes by tuning the voltage amplitude and frequency. This numerical study allows to find the voltage parameters that lead to an efficient trap of the gold nanoparticles. It was shown in [28] that an additional DC voltage in the radial or axial direction shifts the node of the potential in the radial or axial direction. This property shall be used to shift the position of the node in the radial direction r above the planar electrodes. For that purpose, we use additional

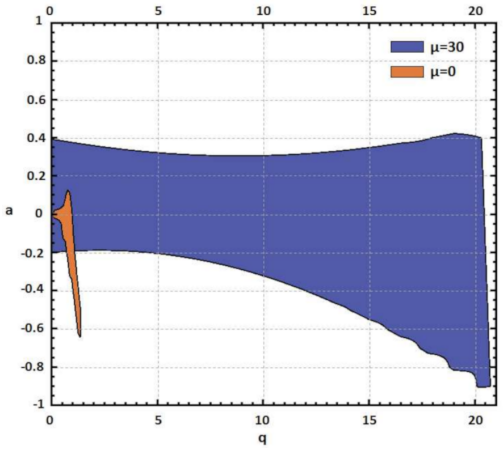

Fig. 2. Stability Diagram. Calculated stability diagram for a charged particle in an oscillating electrical field under vacuum (orange area) and in air (blue area) conditions. a and q are the solutions of the equation of motion of the particle. For this calculation we use a particle of 100 nm diameter of gold placed in air and vacuum conditions.

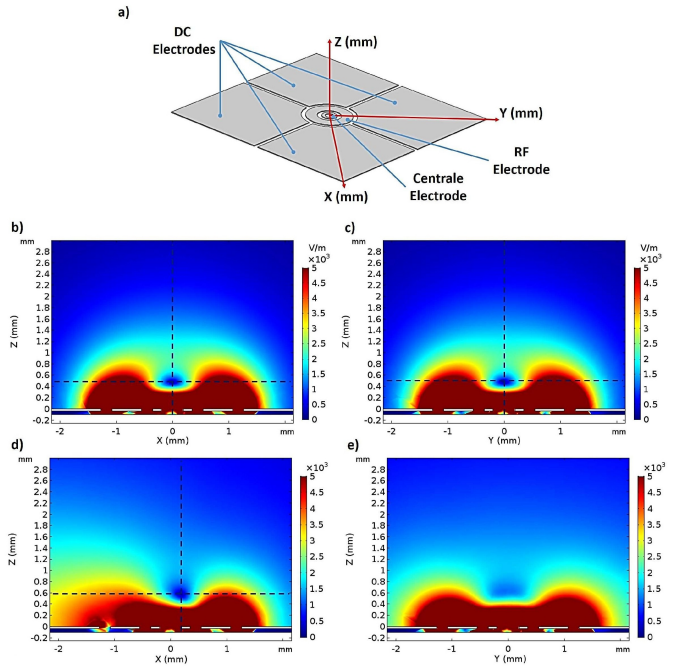

Fig. 3. Electric field maps above the PPT electrode and influence of the DC compensation electrodes. a) Schematic view of the trapping geometry and the different electrodes with the 3 axis definition. b-e) 2D cross sections in the plane XoZ (left row) and YoZ (right row) of the simulated electric field map for 3 different voltage conditions applied on the different electrodes of the PPT :(b,c) RF voltage only, (d,e) RF voltage and one DC electrode at 10V.

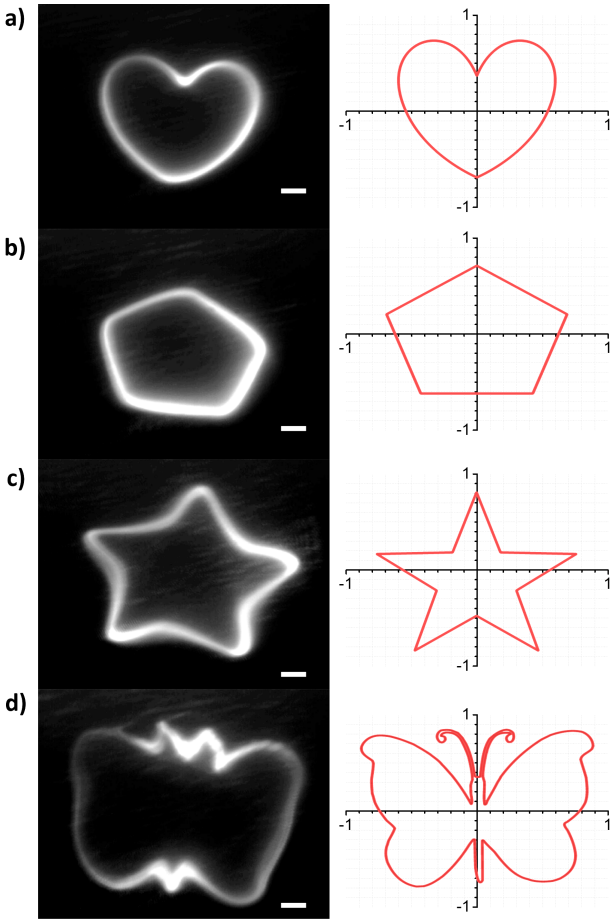

Fig. 4. Free space graphics. Mosaic of images showing the performances of the nanotrap display. On the left side, the image describes the motion of the particle and on the right side the applied trajectory design: (a) heart, (b) pentagon, (c) star and (d) butterfly. We have illuminated the area with a green laser under a diascopic dark-field configuration. The scale bar is 10μm. All the trajectories have been generated under the same conditions: V_{AC}=70 V, $f_{trapping}$=4 kHz, V_{DC}= 9 V, $f_{sampling}$=100kHz. $f_{trapping}$ is the frequency of the applied electrical field while $f_{sampling}$ is the frequency used to scan the points of the particle trajectory. All the images are captured by a coupled objective lens 50$\times$ and a CMOS camera set in POV conditions (50 ms integration time).

DC voltages applied to compensation electrodes. The position of the node in the axial direction can be tuned thanks to the AC voltage. For the radial displacement, the x and y coordinates have first to be discriminated. 4 DC electrodes are placed in the $(0, x, y)$ cartesian coordinates, 2 along the Ox axis at $(-X, 0)$ and $(+X, 0)$, and 2 along the Oy axis at $(0, -Y)$ and $(0, +Y)$ (see Fig.3a). Before manipulating the particles, we study with finite elements method (COMSOL Multiphysics) the possibility to tailor the position of the node of the electric field with voltages, without displacing the electrode. We start with the classical configuration used to trap individual particles above the planar electrode with AC voltage applied to the outer circular electrode (70V, 1kHz). We clearly observe the node of the electric field 0.5mm above the circular electrode, centered on the z axis (Fig.3b,c). On a second step, an additional DC voltage of 10V is applied on a DC electrode along the Ox axis and we can see that the node is displaced along the Ox axis by around 100μm (the scale is in mm) (fgr:fig3d). The height of the node is very slightly increased to 0.6 mm while the distribution of the electric field in the YoZ plane is slightly modified (fgr:fig3e). These simulations confirm the possibility to tailor position of the trap with additional DC voltages without modifying the position of the electrode.

This electronic system allows for a 3D positioning of the particle with a nanometer precision. Our system provides maximum modulation frequencies up to 180 kHz meaning that the time separating two successive points can be as short as 5.5 μsec. We first generate trajectory with a maximum of 4000 points that will behave as pixels of the graphics. The frequency of 100 kHz allows for a scanning of the 4000 pixels of the trajectory in less than 40 milliseconds, *i.e.* in a time much shorter than the POV (roughly around 100 milliseconds). Trajectories of the particle in the (Oxy) plane above the planar electrodes are implemented point by point. For that purpose, we used a computing software (Matlab) and the (x, y) coordinates of the contour plot are extracted directly from a black and white image. This list of the (x, y) pixel coordinates are then converted in polar coordinates (r, θ) and ranked with respect to increasing θ. The ranked coordinates are then converted into voltage values and directly applied to the different electrodes by digital-to-analogue outputs. An example of the treated result with the different directions is presented in Fig.4(a). Each x and y coordinate corresponds to a voltage applied to a pair of electrodes of a given quadrant.

This method is followed to generate different images such

as stars, hearts, rectangles, hexagons,... Each trajectory contains 4000 pixels square and is scanned in 40 milliseconds by a single 100 nm gold particle. The particle is illuminated by a collimated green laser beam and the scattered light is collected (*i*) directly by a webcam (logitech C920) and (*ii*) by a microscope objective (Nikon CFI60 TU plan EPI ELWD 50×, NA=0.6) and imaged onto the CMOS camera. The different images generated with the electrically driven levitated plasmonic particle are displayed in Fig.4 (b-f). The results show the versatility of this electrical approach to tailor the motion of 3D nano-objects at high frequency and accuracy. The technique is also assessed by writing Greek letters. We generated all letters of the Greek alphabet. In a sake of illustration, we assembled different images of letters to form the word FRESNEL (see Fig.5).

Fig. 5. Letters of the Latin alphabet can be obtained with electrically driven plasmonic nanoscatterers. To display the word FRESNEL, each letter is first obtained individually before assembling the 7 images to form the word.

3. CONCLUSION

In conclusion, we showed the ability of planar RF traps manipulate nanoparticles at high frequency and high precision. The position of the particle can be controlled by tuning the applied DC voltage on the four compensation electrodes. The motion dynamics is imposed by the modulation frequency of the electronic card connected to the electrodes (150 kHz). The high frequency allows for driving the particle to 4000 different coordinates in less than 40 milliseconds, a time shorter than the POV. Free-space graphics can therefore be encoded in the trajectory of the particle. The ability of this technique to draw free-space graphics was evidenced by plotting a wide variety of contour plots. Our work shows the proof-of-concept of electrical levitation applied to free-space graphics imaging. The volume of the image depends on the typical size of the electrodes and we anticipate that much larger images could be easily achieved (*i*) by increasing the size of the electrodes from the millimeter range to the centimeter size and (*ii*) by using higher voltage amplifiers than the electronic card to the 4 compensation electrodes that will increase significantly the displacement. Planar RF traps are very stable and can trap a wide range of particle sizes, meaning that this technology has a strong potential to yield large size images entirely driven with electrical voltages.

FUNDING INFORMATION

H2020-MSCA-IF-2015-705616-SMART-LANLIGHT

ACKNOWLEDGMENTS

J.B. is supported by H2020 Marie Skłodowska-Curie Actions fellowship of the European Commission. The authors thank the Fresnel Institute for its financial support through the "Fond pour la Science". The authors thank Jérôme Wenger, Laurent Gallais and Guillaume Baffou for fruitful discussions.

REFERENCES

1. A. Ashkin, J. M. Dziedzic, J. Bjorkholm, and S. Chu, Opt. letters **11**, 288 (1986).
2. A. S. Urban, A. A. Lutich, F. D. Stefani, and J. Feldmann, Nano letters **10**, 4794 (2010).
3. M. L. Juan, M. Righini, and R. Quidant, Nat. Photonics **5**, 349 (2011).
4. J. Gargiulo, I. L. Violi, S. Cerrota, L. Chvátal, E. Cortés, E. M. Perassi, F. Diaz, P. Zemánek, and F. D. Stefani, ACS nano **11**, 9678 (2017).
5. L. Shao and M. Käll, Adv. Funct. Mater. p. 1706272 (2018).
6. D. Foresti, M. Nabavi, M. Klingauf, A. Ferrari, and D. Poulikakos, Proc. Natl. Acad. Sci. **110**, 12549 (2013).
7. D. Foresti and D. Poulikakos, Phys. review letters **112**, 024301 (2014).
8. A. Marzo, S. A. Seah, B. W. Drinkwater, D. R. Sahoo, B. Long, and S. Subramanian, Nat. communications **6**, 8661 (2015).
9. H. Saito, H. Kimura, S. Shimada, T. Naemura, J. Kayahara, S. Jarusirisawad, V. Nozick, H. Ishikawa, T. Murakami, J. Aoki, A. Asano, T. Kimura, M. Kakehata, F. Sasaki, H. Yashiro, M. Mori, K. Torizuka, and K. Ino, Proc. SPIE **6803**, 680309 (2008).
10. Y. Ochiai, T. Hoshi, and J. Rekimoto, ACM Transactions on Graph. (TOG) **33**, 85 (2014).
11. Y. Ochiai, K. Kumagai, T. Hoshi, J. Rekimoto, S. Hasegawa, and Y. Hayasaki, ACM Transactions on Graph. **35**, 17 (2015).
12. M. Martínez-Corral and B. Javidi, Adv. Opt. Photonics **10**, 512 (2018).
13. D. E. Smalley, E. Nygaard, K. Squire, J. V. Wagoner, J. Rasmussen, S. Gneiting, K. Qaderi, J. Goodsell, W. Rogers, M. Lindsey, K. Costner, A. Monk, M. Pearson, B. Haymore, and J. Peatross, Nature **553**, 486 (2018).
14. W. Paul, Rev. Mod. Phys. **62**, 531 (1990).
15. M. Gregor, A. Kuhlicke, and O. Benson, Opt. Express **17**, 24234 (2009).
16. A. Kuhlicke, A. W. Schell, J. Zoll, and O. Benson, Appl. Phys. Lett. **105**, 073101 (2014).
17. A. Kuhlicke, A. Rylke, and O. Benson, Nano Lett. **15**, 1993 (2015).
18. P. Nagornykh, J. E. Coppock, and B. E. Kane, Appl. Phys. Lett. **106**, 244102 (2015).
19. T. Delord, L. Nicolas, Y. Chassagneux, and G. Hétet, Phys. Rev. A **96**, 063810 (2017).
20. J. O. E. C. Oppock, P. A. N. Agornykh, J. A. P. J. M. Urphy, I. S. M. C. A. Dams, S. A. K. Atragadda, and B. E. K. Ane, J. Opt. Soc. Am. B **34**, 36 (2017).
21. G. Planes Conangla, A. W. Schell, R. A. Rica, and R. Quidant, Nano letters **553**, 486 (2018).
22. S. J. Gaskell, "Electrospray: Principles and practice," (1997).
23. C. E. Pearson, D. R. Leibrandt, W. S. Bakr, W. J. Mallard, K. R. Brown, and I. L. Chuang, Phys. Rev. A - At. Mol. Opt. Phys. **73**, 1 (2006).
24. J. Hoffrogge and P. Hommelhoff, New J. Phys. **13** (2011).
25. A. M. Eltony, S. X. Wang, G. M. Akselrod, P. F. Herskind, and I. L. Chuang, Appl. Phys. Lett. **102** (2013).
26. I. Alda, J. Berthelot, R. A. Rica, and R. Quidant, Appl. Phys. Lett. **109** (2016).
27. M. Nasse and C. Foot, Eur. J. Phys. **22**, 563 (2001).
28. P. F. Herskind, A. Dantan, M. Albert, J. P. Marler, and M. Drewsen, J. Phys. B: At. Mol. Opt. Phys. **42**, 154008 (2009).

REFERENCES

1. A. Ashkin, J. M. Dziedzic, J. Bjorkholm, and S. Chu, "Observation of a single-beam gradient force optical trap for dielectric particles," Opt. letters **11**, 288 (1986).
2. A. S. Urban, A. A. Lutich, F. D. Stefani, and J. Feldmann, "Laser printing single gold nanoparticles," Nano letters **10**, 4794 (2010).
3. M. L. Juan, M. Righini, and R. Quidant, "Plasmon nano-optical tweezers," Nat. Photonics **5**, 349 (2011).
4. J. Gargiulo, I. L. Violi, S. Cerrota, L. Chvátal, E. Cortés, E. M. Perassi, "Accuracy and Mechanistic Details of Optical Printing of Single Au and Ag Nanoparticles," F. Diaz, P. Zemánek, and F. D. Stefani, ACS nano **11**, 9678 (2017).
5. L. Shao and M. Käll, "Light-Driven Rotation of Plasmonic Nanomotors," Adv. Funct. Mater. p. 1706272 (2018).
6. D. Foresti, M. Nabavi, M. Klingauf, A. Ferrari, and D. Poulikakos, "Acoustophoretic contactless transport and handling of matter in air," Proc. Natl. Acad. Sci. **110**, 12549 (2013).
7. D. Foresti and D. Poulikakos, "Acoustophoretic contactless elevation, orbital transport and spinning of matter in air," Phys. review letters **112**, 024301 (2014).
8. A. Marzo, S. A. Seah, B. W. Drinkwater, D. R. Sahoo, B. Long, and S. Subramanian, "coustophoretic contactless elevation, orbital transport and spinning of matter in air," Nat. communications **6**, 8661 (2015).
9. H. Saito, H. Kimura, S. Shimada, T. Naemura, J. Kayahara, S. Jarusirisawad, V. Nozick, H. Ishikawa, T. Murakami, J. Aoki, A. Asano, T. Kimura, M. Kakehata, F. Sasaki, H. Yashiro, M. Mori, K. Torizuka, and K. Ino, "Laser-plasma scanning 3D display for putting digital contents in free space," Proc. SPIE **6803**, 680309 (2008).
10. Y. Ochiai, T. Hoshi, and J. Rekimoto, "Pixie dust: graphics generated by levitated and animated objects in computational acoustic-potential field" ACM Transactions on Graph. (TOG) **33**, 85 (2014).
11. Y. Ochiai, K. Kumagai, T. Hoshi, J. Rekimoto, S. Hasegawa, and Y. Hayasaki, "Fairy Lights in Femtoseconds: Aerial and Volumetric Graphics Rendered by Focused Femtosecond Laser Combined with Computational Holographic Fields," ACM Transactions on Graph. **35**, 17 (2015).
12. M. Martínez-Corral and B. Javidi, "Fundamentals of 3D imaging and displays: a tutorial on integral imaging, light-field, and plenoptic systems," Adv. Opt. Photonics **10**, 512 (2018).
13. D. E. Smalley, E. Nygaard, K. Squire, J. V. Wagoner, J. Rasmussen, S. Gneiting, K. Qaderi, J. Goodsell, W. Rogers, M. Lindsey, K. Costner, A. Monk, M. Pearson, B. Haymore, and J. Peatross, "A photophoretic-trap volumetric display," Nature **553**, 486 (2018).
14. W. Paul, "Electromagnetic traps for charged and neutral particles," Rev. Mod. Phys. **62**, 531 (1990).
15. M. Gregor, A. Kuhlicke, and O. Benson, "Soft-landing and optical characterization of a preselected single fluorescent particle on a tapered optical fiber," Opt. Express **17**, 24234 (2009).
16. A. Kuhlicke, A. W. Schell, J. Zoll, and O. Benson, "Nitrogen vacancy center fluorescence from a submicron diamond cluster levitated in a linear quadrupole ion trap," Appl. Phys. Lett. **105**, 073101 (2014).
17. A. Kuhlicke, A. Rylke, and O. Benson, "On-demand electrostatic coupling of individual precharacterized nano- and microparticles in a segmented Paul trap," Nano Lett. **15**, 1993 (2015).
18. P. Nagornykh, J. E. Coppock, and B. E. Kane, "Cooling of levitated graphene nanoplatelets in high vacuum," Appl. Phys. Lett. **106**, 244102 (2015).
19. T. Delord, L. Nicolas, Y. Chassagneux, and G. Hétet, "Strong coupling between a single nitrogen-vacancy spin and the rotational mode of diamonds levitating in an ion trap," Phys. Rev. A **96**, 063810 (2017).
20. J. O. E. C. Oppock, P. A. N. Agornykh, J. A. P. J. M. Urphy, I. S. M. C. A. Dams, S. A. K. Atragadda, and B. E. K. Ane, "Dual-trap system to study charged graphene nanoplatelets in high vacuum," J. Opt. Soc. Am. B **34**, 36 (2017).
21. G. Planes Conangla, A. W. Schell, R. A. Rica, and R. Quidant, "Motion control and optical interrogation of a levitating single NV in vacuum," Nano letters **553**, 486 (2018).
22. S. J. Gaskell, "Electrospray: Principles and practice," (1997).
23. C. E. Pearson, D. R. Leibrandt, W. S. Bakr, W. J. Mallard, K. R. Brown, and I. L. Chuang, "Experimental investigation of planar ion traps," Phys. Rev. A - At. Mol. Opt. Phys. **73**, 1 (2006).
24. J. Hoffrogge and P. Hommelhoff, "Planar microwave structures for electron guiding," New J. Phys. **13** (2011).
25. A. M. Eltony, S. X. Wang, G. M. Akselrod, P. F. Herskind, and I. L. Chuang, "Transparent ion trap with integrated photodetector," Appl. Phys. Lett. **102** (2013).
26. I. Alda, J. Berthelot, R. A. Rica, and R. Quidant, "Trapping and manipulation of individual nanoparticles in a planar Paul trap," Appl. Phys. Lett. **109** (2016).
27. M. Nasse and C. Foot, "Influence of background pressure on the stability region of a Paul trap," Eur. J. Phys. **22**, 563 (2001).
28. P. F. Herskind, A. Dantan, M. Albert, J. P. Marler, and M. Drewsen, "Positioning of the rf potential minimum line of a linear Paul trap with micrometer precision," J. Phys. B: At. Mol. Opt. Phys. **42**, 154008 (2009).